1 Scientific Justification

1.1 Introduction

Luminosity is a basic observable quasar parameter, directly linked to fundamental physical quantities like the accretion rate onto and mass of the central super-massive black hole. The extreme luminosity of quasars helps to drive high-velocity outflows which chemically enrich the host galaxy ISM and IGM, and may also regulate star formation in merging systems via blowout. To obtain a complete picture of quasars, we must understand how these fundamental parameters drive observable ones like luminosity. The black hole mass and accretion rate most directly affect the X-ray through optical luminosity of quasars, but quasars emit across the entire electromagnetic spectrum. While quasar spectral energy distributions generally peak in the optical-ultraviolet regime where the putative accretion disk emits most strongly, the mid-to-far infrared is often similarly strong. The mid-infrared (MIR) emission is thought to come from dust heated by the quasar's shorter wavelength radiation, and provides information about the distribution of gas and dust surrounding the central engine.

The ratio of optical-to-mid-infrared emission increases with increasing luminosity (e.g., Maiolino et al. 2007) consistent with ideas of a "receding torus" where the distance to, and structure of, the torus is driven by the X-ray to optical luminosity (Lawrence 1991). The covering fraction of dust around the central engine appears to depend strongly on luminosity.

Longer wavelengths, beyond 20 μm rest-frame, are thought to be dominated by emission from cooler dust heated by star formation activity (e.g., Shi et al. 2007; Netzer et al. 2007), at least in lower luminosity quasars. It has been difficult to study this part of the spectrum in the most luminous quasars, as they are only found at high redshifts ($z > 1$ or so), and the rest-frame spectrum is redshifted to longer wavelengths. *Spitzer* IRS spectra have shown rich features in the 5–38 μm region for low-redshift quasars (Fig. 1), but at high redshifts only shorter rest wavelengths are seen, and some important features are not seen in the most luminous quasars. For instance, PAH features emitted from star formation regions vanish, presumably because their strength does not increase as fast as the quasar-heated dust emission (e.g., Maiolino et al. 2007). Prominent broad silicate features around 10 and 18 μm are not fully probed either with the restricted rest wavelength range.

Other recent studies on high-redshift and/or high-luminosity quasars tried to use IRAC and MIPS photometry to cover a wider wavelength range (Hines et al. 2006; Richards et al. 2006; Gallagher et al. 2007). However, the longest wavelength in those studies is MIPS 70 μm (rest-frame 20 μm at $z = 2.5$), still not long enough for studying cool dust likely powered by star formation. Only shorter wavelength mid-infrared emission has been studied properly in luminous quasars. We propose to observe a sample of the most luminous quasars in the universe that already has mutli-wavelength data in order to obtain the SED of the most extreme quasars.

1.2 Investigation of the Most Luminous Quasars with *Spitzer*

1.2.1 Our Sample and Plan

We will use IRS (4 low-resolution modes, 5–38 μm) and MIPS (24, 70, 160 μm) to study a representative sample of 28 of the most luminous quasars. The IRS spectra cover the rest-frame 10 μm silicate and 7.7 μm PAH features, while the MIPS observations measure

the amount of emission from cool dust.

Our targets are from the "core" sample of Just et al. (2007), excluding lensed and BAL quasars. More specifically, they selected the most luminous quasars from SDSS DR3 with $M_i < -29.28$ (Fig. 2); we exclude their extended NED sample of $z \geq 4$ quasars since the higher redshifts limit the rest-wavelength range we can probe with *Spitzer*. Just et al. (2007) presented X-ray properties of these quasars and refined how the optical-to-X-ray ratio changes with changing luminosity when comparing with low-to-moderate luminosity quasars (Strateva et al.2005; Steffen et al. 2006; Shemmer et al. 2006). In addition to the SDSS and X-ray data, these sources have radio and near-IR data as well.

This sample is uniformly defined, large enough for statistical studies, and bright enough for a practical *Spitzer* request. In the same way Just et al. (2007) established the X-ray properties of the most luminous qusars, we will establish the same for the MIR.

These are among the most optically luminous quasars in the universe. Even assuming they are radiating near the Eddington limit, their luminosity requires a black hole mass of order $10^9 - 10^{10} M_\odot$, putting them at the high end of the known quasar black hole masses. As the most luminous quasars, they are likely to have both the largest black hole masses and the largest accretion rates, and to be hosted in the most massive galaxies being formed in the most massive universal overdensities. These objects have presumably evolved into giant elliptical galaxies we see locally today. Therefore, our sample is also ideal for studying evolution as it has a relatively narrow luminosity range ($-30.24 < M_i < -29.28$) but spans the redshift range where these objects exist in the universe.

So far, little is known empirically about the star formation associated with the most luminous quasars. Based on lower luminosity AGNs and quasars, star formation seems to correlate with the intensity of the nuclear activity (e.g., Schweitzer et al. 2006, Shi et al. 2007). Much less is known about how this correlation develops at higher luminosities, with some evidence that the star formation rate saturates (e.g., Maiolino et al. 2007). This information is crucial to understanding the evolution of galaxies and the connection to black hole growth. We should establish the relationship in the most extreme objects as the first test of theoretical notions. The black hole mass and Eddington accretion ratio can be estimated using the UV/optical continuum and emission lines (e.g., C IV or Mg II which are covered in the SDSS spectra, Vestergaard et al. 2002; Dietrich & Hamann 2004). The star-formation rate in the most luminous quasars can be gauged by the amount of PAH and cool dust emission. Therefore we have to go to longer rest-frame wavelengths in the MIR.

Our first goal is to establish the dust temperature distribution using MIR spectra and colors, to obtain MIR relative strength compared to the optical emission, and to look for relationships with black hole mass and accretion rate, both within the sample and in comparison with lower luminosity objects available in the archives and literature.

As shown clearly in Figure 1, quasar MIR spectra vary greatly from object to object, and for individual objects, even the continuum slope often changes dramatically from shorter wavelengths to longer wavelengths. Other high luminosity *Spitzer* surveys used IRS, IRAC, or MIPS without 160 μm data, but at high redshift, this does not go to rest-frame wavelengths long enough for proper comparisons or to probe cooler stellar-heated dust. To investigate cool dust, we are required to have 160 μm as well as 70 μm observations, and our sample is the best, most luminous sample with which to do this.

Other existing samples of nearly comparable luminosity do not have the 160 μm data because of the observational expense. While *Spitzer* is available, this should be done. The present sample is the easiest high-redshift sample for which the long-wavelength data may be

obtained. Without it, we cannot properly compare the high luminosity quasars with those at low redshift that have been studied so extensively. Moreover, unlike most quasar samples, including high-z, high-luminosity *Spitzer* samples, this unique sample also has the X-ray data, similarly difficult to obtain as the infrared data, as well as optical, NIR (2MASS), radio (NVSS & FIRST) and some UV (GALEX) data. It's now or never to do this right for the easiest and most extreme high-z sample.

The redshifts of this and other high-luminosity samples allow IRS to probe the rest-frame 1–10 μm regime, which includes the suggested MIR enhancement from hot dust between 3–5 μm that increases with luminosity (Richards et al. 2006; Gallagher et al. 2007). The huge luminosity of these objects must have other tremendous impacts on the dust and dusty environment surrounding the central engine. This is the extreme and possibly the best case to compare with theoretical models in order to understand the properties of the dusty regions, including temperature, structure, and radius (Gallagher et al. 2007).

1.2.2 SEDs of the Most Luminous Quasars

One clear benefit of this sample is that multi-wavelength data can be collected more effectively due to its high luminosity. Therefore it is easy to build SEDs of this extreme type of objects for the community, which we will supply on our website (http://physics.uwyo.edu/agn). We have other SEDs already disseminated from that page.

All objects have SDSS spectra and 2MASS data. Radio observations are available from NVSS (Condon et al. 1998) and FIRST (Becker et al. 1995). More importantly, all objects have X-ray data from *Chandra*, *ROSAT*, or *XMM-Newton*, which have been systematically analyzed (Just et al. 2007). The only missing part, which is a very important part, is the MIR information. Adding IRS and MIPS observations, we will be able to build SEDs covering the entire electromagnetic spectrum for this most luminous quasar sample.

Quasar SED changes with luminosity (Gallagher et al. 2007; Just et al. 2007). The mean SED of this sample will enable us to fix the spectral properties at one extreme end. Archival data provides the other extreme for lower-luminosity quasars. The multi-wavelength data can probe from the inner-most region of the accretion disk, to the emission line region, and to the large-scale dusty environment. They enable us to study the connections between the regions and to obtain a complete, better picture of the most luminous quasars.

Individual SEDs will be used to obtain the true bolometric luminosity of the objects, and help to establish a better bolometric correction for objects without multi-wavelength data. There is an important issue that needs to be studied: double counting. The infrared photons are generally thought to be reprocessed optical/UV photons from the AGN or stellar sources. A controversy exists about how to estimate the bolometric luminosity — while including the infrared needs to take into account reprocessing in a realistic way, ignoring the infrared must make assumptions about the emission of optical/UV photons as a function of viewing angle. Multi-wavelength data without a MIR gap give us a better chance to attack this issue and find a better way of determining bolometric corrections.

1.3 Summary

While a cooled *Spitzer* is available, we propose to establish the SEDs of the most luminous quasars in the universe. This has not yet been well done, particularly at the wavelengths that probe dust heated by star formation. This sample represents an extreme of parameter space and relatively easy observations that should be conducted while possible.

2 Technical Plan

Our sample has 28 of the most luminous quasars selected from SDSS DR3 (see Scientific Justification for details). We propose to observe them using IRS 4 low-resolution bands in staring mode and 3 MIPS bands in enhanced photometry mode. Two objects have been observed in one IRS low-resolution band (19.5–38.0 μm) and we do not propose repeat observations.

The visibility windows for these targets within an year after June 2008 are all large, with a minimum total duration of 80 days. We are submitting the final AORs for this program. We request a total observing time of 39.9 hours, including 7.4 hours for IRS and 32.5 hours for MIPS.

2.1 Estimate of Flux Density and Background

The EX-PET is not designed specifically for the IRS bands. Moreover, the only AGN SED template "Seyfert 2" is not suitable for our broad-line objects (It over-estimates type 1 AGN flux densities and this is probably why 160 μm is not detected in some previous high-z, high-luminosity quasar studies). Therefore, we built our own Estimation Tool using a mean SED for radio-quiet quasars from Elvis et al. (1994; lacking more appropriate SEDs) and estimated the observed flux densities at the IRS and MIPS bands using the redshifts and SDSS i-band magnitudes for our targets. For IRS, the flux densities were estimated at the default fiducial wavelengths in SPEC-PET (6.9, 10.85, 18.0, 30.3 μm).

We used SPOT to estimate the backgrounds at all bands for each target. We tried to get a better "standard" to assess background levels at the IRS bands. We used the low, medium and high background values at different bands (http://ssc.spitzer.caltech.edu/obs/bg.html) and simple interpolation to get the corresponding values for IRS bands. Our estimates are listed in Table 1 along with the backgrounds for other bands from the above SSC website. This "standard" was used to assess the background values of our targets in terms of low, medium, or high, which is needed to estimate exposure time. The estimated flux density and background are listed in the Observation Summary Table (§5).

Table 1: Low, Medium, and High Backgrounds at Different Wavelengths

Wavelength	Background (mJy/sr)		
(μm)	Low	Medium	High
3.6	0.0769	0.125	0.43
4.5	0.267	0.366	0.85
5.8	1.37	1.93	4.64
6.9	**3.42**	**4.81**	**11.5**
8.0	5.47	7.69	18.3
10.85	**9.64**	**13.8**	**34.8**
15.75	16.8	24.4	63.1
18.00	**16.8**	**24.5**	**64.5**
22.25	16.7	24.7	67.0
24.00	16.1	23.9	65.6
30.30	**14.6**	**21.9**	**61.0**
70.00	5.15	8.95	32.3
160.0	6.53	16.5	84.3

Note.— Values in bold face are interpolations for the fiducial wavelengths of IRS low-resolution bands.

2.2 IRS staring

In order to perform meaningful spectral analyses and separate the MIR continuum from emission/absorption features such as the 10 μm silicate feature, we require a continuum S/N$\geq$8 in the 4 IRS bands. We use our estimated flux, background assessment and SPEC-

PET to estimate the exposure time needed to reach the S/N. The Ramp Duration, Number of Cycles, and S/N are also listed in the Observation Summary Table (§5). When different combinations of ramp duration and number of cycles give similar total integration time (e.g., 30×4 vs. 120×1) for our requested S/N, we always choose the one with longer ramp duration and this usually gives us a slightly higher S/N and shorter AOR duration.

We used SPOT to choose PCRS peak-up stars for our targets. This guarantees high accuracy target placement on the slits and better photometric calibration. We have verified that there is no bright neighbor for these peak-up stars.

2.3 MIPS photometry

We use our estimated flux, background assessment and EX-PET to estimate the exposure time needed for a certain S/N. At 24 μm, the minimum exposure time (ramp duration of 3 seconds with a single cycle) can easily reach a S/N above 20 for our targets. At 70 μm, we want accurate photometry to compensate for the lack of spectral information and try to match the S/N$\geq$8 of IRS. For most objects, this only requires the exposure time from the the minimum of $\sim$ 6 min (ramp duration of 3 seconds with one cycle) to about 10 minutes.

As our targets are essentially point sources, we take advantage of the the new 160 μm enhanced photometry mode for small field which can improve both the repeatability and sensitivity by 15–20%.

MIPS 160 μm needs to be done in cold campaigns. We need 160 μm, because it is critical for our science to understand the properties of the cold dust in the high-redshift, most luminous quasars. We need to do better than just detection and require a S/N$\geq$4 to be cost-effective without compromising our science. We will be able to define a better color or continuum slope when combined with other data. The S/N for one object (ID 08 in Observation Summary Tables) can only reach 3.5 even with the maximum number of cycles (20) in one AOR. For 4 other objects (ID 07, 20, 21, 24) that cannot reach S/N=4 within 20 cycles, we also drop the S/N back to 3.5 to be cost effective. Our choice of the enhanced photometry mode should actually allow us to do better.

2.4 Data Analysis

The data analyses will be done mainly at the University of Wyoming under the direction of the PI who actively leads an AGN group already working with IRS and MIPS data of earlier GO programs (GO-2, #20084, GO-3, #33075).

We will use the pipelined products from the SSC. However, additional processing of the data will be required. We will use the SMART package to re-extract and recalibrate the IRS spectra, and MOPEX to work on the MIPS data. Additional analysis will be performed with standard procedures in IRAF and custom procedures written in IDL.

Co-I Z. Shang has been working with *Spitzer* data and is familiar with both IRS and MIPS data. Co-I D. Hines is a member of the MIPS instrument teams, and is also an expert in IRS and IRAC data reduction. Co-I O. Shemmer is an expert in IR astronomy and is also very familiar with *Spitzer* data.

We will investigate the properties of the cold dust likely powered by star formation in the most luminous quasars, and compare these with local quasars. We will construct the SEDs of the most luminous quasars and make them available to the AGN community. We will make statistical comparisons of the quasar spectral properties in different wavebands. Our Co-Is defined the sample (Just et al. 2007) and have extensive experience in X-ray and multi-wavelength studies.

3 Legacy Data Products Plan

4 Figures and Tables

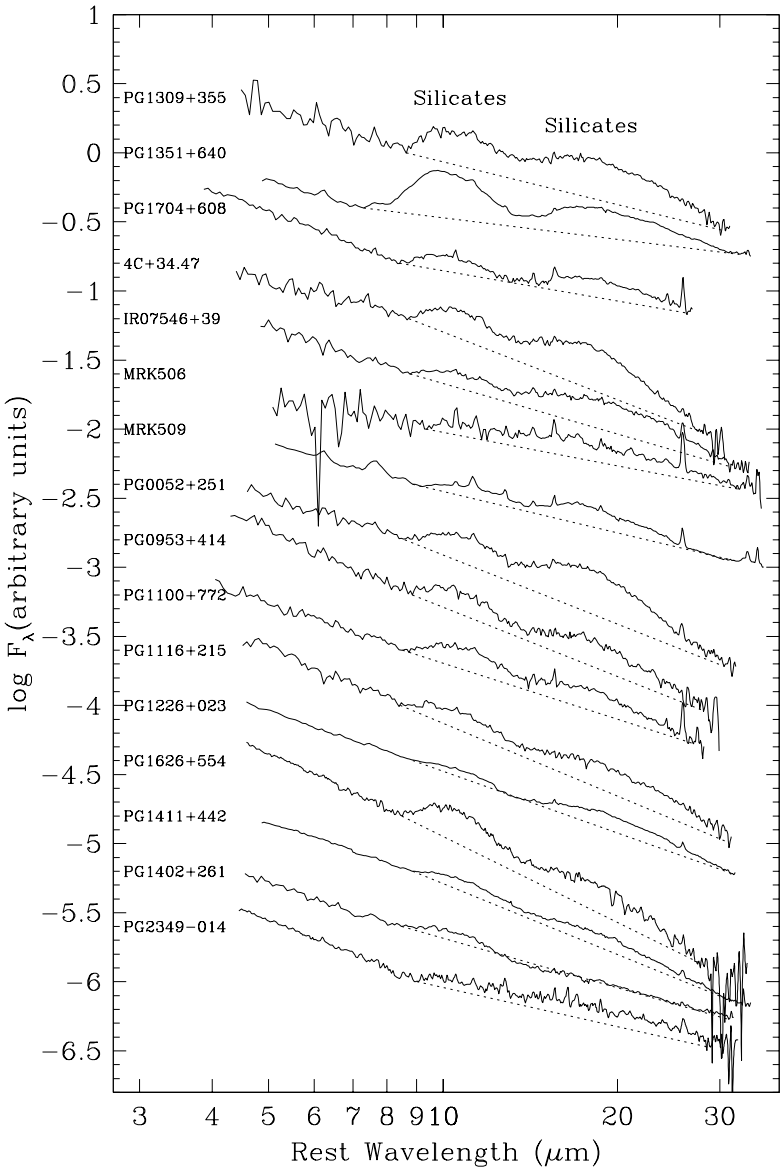

Figure 1: IRS spectra of low-redshift type 1 quasars from archive and our previous program. Data at longer wavelengths are important as the dotted lines show that the continuum slope at longer wavelengths does not necessarily agree with the continuum slope below $\sim 8\,\mu$m.

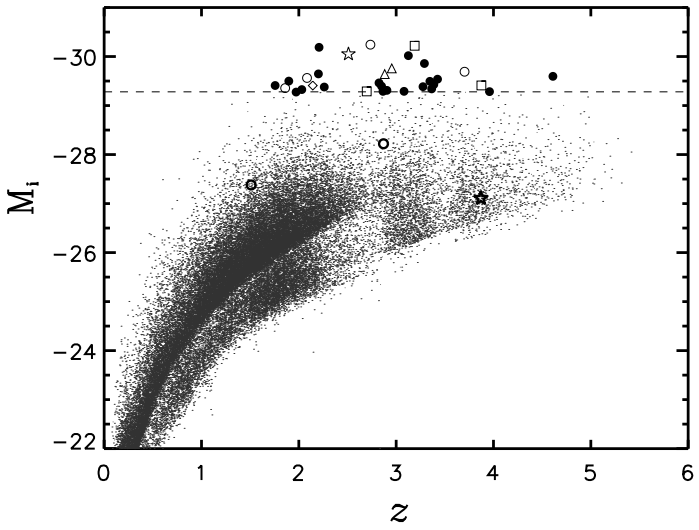

Figure 2: Sample selection from Just et al. (2007), showing absolute i-band magnitude vs. redshift for the SDSS sample compared with the SDSS DR3 quasar catalog. The dashed line indicates the cutoff at $M_i = -29.28$. Objects below the dashed line are lensed quasars that have been deamplified and removed from the sample.

5 Observation Summary Table

There are 7.4 hours total in IRS AORs, and 32.5 hours total in MIPS AORs.

Observation Summary for IRS

				1st line: Estimated Flux Density (mJy) 2st line: Background (mJy/sr) (High/Medium/Low) 3rd line: Ramp Duration × Cycles (S/N)			
obj	Object Name	z	i (mag)	SL2 (6.9 μm)	SL1 (10.85 μm)	LL2 (18.0 μm)	LL1(30.3 μm)
01	SDSSJ012156.04+144823.9	2.859	16.99	2.0	4.3	7.2	13.
				3.54-9.07 (H)	17.3-37.7 (H)	32.7-62.0 (H)	29.3-50.5 (H)
				60 x 1 (9.8)	14 x 1 (8.4)	120 x 1 (10)	30 x 2 (9.3)
02	SDSSJ020950.71-000506.4	2.852	16.84	2.3	4.9	8.3	15.
				3.65-7.84 (H)	17.9-32.8 (H)	33.4-54.1 (H)	29.4-44.0 (H)
				60 x 1 (11)	14 x 1 (9.6)	30 x 2 (8.2)	30 x 2 (11)
03	SDSSJ073502.31+265911.4	1.974	16.16	5.6	9.8	17.	31.
				3.79-9.22 (H)	18.5-38.9 (H)	35.0-64.9 (H)	31.4-53.4 (H)
				14 x 1 (8.8)	6 x 1 (10)	30 x 1 (12)	14 x 1 (10)
04	SDSSJ075054.64+425219.2	1.896	15.85	7.7	13.	22.	42.
				3.13-7.14 (H)	14.4-28.5 (H)	25.6-44.9 (H)	21.9-35.3 (H)
				14 x 1 (12)	6 x 1 (13)	14 x 1 (10)	6 x 1 (8.6)
05	SDSSJ080342.04+302254.6	2.031	16.15	5.6	9.9	17.	32.
				3.64-8.77 (H)	17.5-36.7 (H)	32.8-60.4 (H)	29.1-49.3 (H)
				14 x 1 (8.8)	6 x 1 (10)	30 x 1 (12)	14 x 1 (11)
06	SDSSJ090033.49+421546.8	3.290	16.68	2.3	5.4	9.4	17.
				3.09-6.68 (H)	14.2-26.6 (H)	25.0-41.7 (H)	21.2-32.6 (H)
				60 x 1 (11)	14 x 1 (10)	30 x 2 (9.3)	30 x 1 (8.5)
07	SDSSJ094202.04+042244.5	3.276	17.16	1.5	3.5	6.	11.
				3.50-8.54 (H)	16.6-35.7 (H)	30.6-58.6 (H)	27.0-47.5 (H)
				60 x 2 (10)	14 x 2 (9.8)	120 x 1 (8.5)	120 x 1 (11)
08	SDSSJ095014.05+580136.5	3.960	17.61	0.8	2.	3.9	6.8
				2.58-4.91 (M)	11.3-18.9 (H)	19.0-28.5 (M)	15.5-21.7 (M)
				240 x 1 (11)	60 x 1 (9.5)	120 x 1 (8.6)	120 x 1 (10)
09	SDSSJ100129.64+545438.0	1.756	15.67	9.5	16.	27.	51.
				2.64-5.03 (M)	11.7-19.5 (H)	19.7-29.5 (M)	16.1-22.5 (M)
				14 x 1 (15)	6 x 1 (16)	6 x 1 (11)	6 x 1 (13)
10	SDSSJ101447.18+430030.1	3.126	16.39	3.1	7.2	12.	22.
				2.99-5.87 (H)	13.5-23.2 (H)	23.3-35.9 (H)	19.5-27.8 (H)
				60 x 1 (15)	14 x 1 (14)	30 x 1 (8.3)	30 x 1 (11)
11	SDSSJ110610.73+640009.6	2.203	15.96	6.3	12.	19.	37.
				2.47-4.26 (M)	10.6-16.3 (H)	17.5-24.3 (M)	13.8-18.3 (M)
				14 x 1 (10)	6 x 1 (12)	6 x 1 (8.1)	6 x 1 (10)
12	SDSSJ111038.64+483115.6	2.955	16.53	2.9	6.4	11.	20.
				2.78-4.94 (M)	12.2-19.2 (H)	20.6-29.1 (M)	16.9-22.3 (M)
				60 x 1 (15)	14 x 1 (12)	30 x 1 (12)	14 x 1 (9.3)
13	SDSSJ121930.77+494052.3	2.699	16.79	2.5	5.2	8.7	16.
				2.71-4.33 (M)	11.7-16.7 (H)	19.5-25.2 (M)	15.8-19.1 (M)
				60 x 1 (13)	14 x 1 (10)	30 x 1 (9.2)	30 x 1 (11)
14	SDSSJ123549.47+591027.0	2.825	16.71	2.6	5.6	9.3	17.
				2.57-3.94 (M)	11.0-15.1 (H)	17.9-22.5 (M)	13.6-16.9 (M)
				60 x 1 (14)	14 x 1 (11)	30 x 1 (9.9)	14 x 1 (8)
15	SDSSJ123641.46+655442.0	3.387	17.17	1.4	3.4	6.	11.
				2.57-3.86 (M)	10.7-14.6 (M)	16.8-21.7 (M)	12.7-16.3 (M)
				60 x 2 (11)	14 x 1 (8.5)	30 x 2 (9.1)	30 x 1 (8)
16	SDSSJ135044.67+571642.8	2.906	16.92	2.1	4.6	7.7	14.
				2.63-3.55 (L)	11.2-13.6 (M)	17.4-20.2 (M)	13.1-15.2 (L)
				60 x 1 (11)	14 x 1 (11)	30 x 1 (8.2)	30 x 1 (11)
17	SDSSJ140747.22+645419.9	3.082	17.07	1.7	3.8	6.6	12.
				2.68-3.47 (L)	10.7-13.1 (M)	15.9-19.5 (M)	11.9-14.6 (L)
				60 x 1 (9.2)	14 x 1 (9.4)	30 x 2 (10)	30 x 1 (9.5)
18	SDSSJ142123.98+463317.8	3.363	17.22	1.3	3.2	5.7	10.
				2.63-3.62 (M)	11.3-13.6 (M)	18.6-20.4 (M)	14.7-15.7 (M)
				60 x 2 (9.9)	14 x 1 (8)	30 x 2 (8.7)	30 x 2 (10)

Observation Summary for IRS (continued)

obj	Object Name	z	i (mag)	1st line: Estimated Flux Density (mJy) 2st line: Background (mJy/sr) (High/Medium/Low) 3rd line: Ramp Duration × Cycles (S/N) SL2 (6.9 μm)	SL1 (10.85 μm)	LL2 (18.0 μm)	LL1(30.3 μm)
19	SDSSJ142656.17+602550.8	3.192	16.22	3.6 2.69-3.36 (L) 14 x 2 (8.4)	8.3 11.1-12.8 (M) 6 x 1 (10)	14. 16.5-19.0 (M) 14 x 1 (9.8)	26. 12.3-14.6 (L) archive
20	SDSSJ143835.95+431459.2	4.611	17.64	0.7 2.62-3.75 (M) 240 x 1 (9.3)	1.7 11.3-14.1 (M) 60 x 1 (12)	3.7 18.6-20.9 (M) 120 x 1 (8.2)	6.2 14.6-16.0 (M) 120 x 1 (9.4)
21	SDSSJ144542.75+490248.9	3.876	17.48	0.92 2.65-3.51 (L) 60 x 3 (8.8)	2.3 11.2-13.1 (M) 14 x 2 (8.2)	4.4 18.3-19.3 (M) 120 x 1 (9.7)	7.7 13.8-15.2 (L) 30 x 2 (8.7)
22	SDSSJ152156.48+520238.4	2.208	15.43	10. 2.69-3.36 (L) 14 x 1 (15)	19. 11.2-12.5 (M) 6 x 1 (22)	32. 16.8-18.8 (M) 6 x 1 (13)	60. 12.7-14.7 (L) 6 x 1 (16)
23	SDSSJ161434.67+470420.0	1.860	15.86	7.7 2.62-3.58 (L) 14 x 1 (12)	13. 10.5-13.3 (M) 6 x 1 (15)	22. 15.8-19.5 (M) 6 x 1 (9.3)	42. 11.9-14.5 (L) 6 x 1 (12)
24	SDSSJ162116.92-004250.8	3.703	17.24	1.2 3.20-7.15 (H) 60 x 2 (8.4)	3. 14.5-28.3 (H) 14 x 2 (8.5)	5.6 26.0-44.5 (H) 120 x 2 (11)	9.7 22.5-35.1 (H) 120 x 1 (10)
25	SDSSJ170100.62+641209.0	2.735	15.89	5.7 2.62-3.22 (L) 14 x 1 (9.2)	12. 9.90-12.5 (M) 6 x 1 (14)	20. 14.6-18.8 (M) 6 x 1 (8.5)	37. 10.9-14.3 (L) 6 x 1 (11)
26	SDSSJ173352.22+540030.5	3.425	17.11	1.5 2.37-3.54 (L) 60 x 1 (8.1)	3.5 9.36-13.0 (M) 14 x 1 (8.7)	6.3 14.3-18.9 (M) 30 x 2 (9.6)	11. 10.8-14.1 (L) archive
27	SDSSJ212329.46-005052.9	2.262	16.35	4.3 3.16-7.72 (H) 14 x 2 (9.7)	8.1 14.9-31.6 (H) 6 x 1 (8.6)	13. 27.2-50.8 (H) 30 x 1 (9)	26. 23.7-40.5 (H) 14 x 1 (8.7)
28	HS1603+3820	2.510	15.89	6.1 2.46-3.92 (M) 14 x 1 (9.8)	12. 10.6-14.7 (M) 6 x 1 (14)	20. 17.1-21.7 (M) 6 x 1 (8.5)	38. 13.0-16.2 (M) 6 x 1 (10)

Note:— Flux density and background are estimated at the listed fiducial wavelengths (SPECPET default values) for the 4 IRS bands. Please see Table 1 for our assessment of the background level (H/M/L). The i(mag) is the SDSS i-band magnitude. For HS1603+3820, it is chosen to be the same as that of one object with similar redshift and 2MASS magnitudes.

Observation Summary for MIPS

obj	Object Name	z	i (mag)	1st line: Estimated Flux Density (mJy) 2st line: Background (mJy/sr) (High/Medium/Low) 3rd line: Ramp Duration × Cycles (S/N) (24 μm)	(70 μm)	(160 μm)
01	SDSSJ012156.04+144823.9	2.859	16.99	9.9 33.0-59.1 (H) 3 x 1 (46)	29. 11.2-17.3 (H) 10 x 3 (7.9)	35. 8.67-9.82 (M) 10 x 16 (3.9)
02	SDSSJ020950.71-000506.4	2.852	16.84	11. 33.4-51.6 (H) 3 x 1 (51)	33. 10.7-14.8 (H) 10 x 3 (9)	40. 6.12-6.88 (L) 10 x 10 (4.2)
03	SDSSJ073502.31+265911.4	1.974	16.16	24. 35.4-62.3 (H) 3 x 1 (110)	55. 12.0-18.4 (H) 10 x 1 (8.7)	57. 9.29-10.5 (M) 10 x 6 (4.)
04	SDSSJ075054.64+425219.2	1.896	15.85	32. 25.1-41.9 (H) 3 x 1 (150)	73. 8.24-11.9 (H) 3 x 2 (10)	74. 7.61-8.30 (M) 10 x 4 (4.1)
05	SDSSJ080342.04+302254.6	2.031	16.15	24. 32.9-57.6 (H) 3 x 1 (110)	56. 10.9-16.7 (H) 10 x 1 (8.8)	59. 7.50-8.60 (M) 10 x 6 (4.)
06	SDSSJ090033.49+421546.8	3.290	16.68	13. 24.4-38.8 (H) 3 x 1 (61)	39. 7.65-10.7 (H) 10 x 2 (8.7)	50. 5.40-5.97 (L) 10 x 6 (4.)
07	SDSSJ094202.04+042244.5	3.276	17.16	8.2 30.7-55.7 (H) 3 x 1 (38)	25. 10.1-16.0 (H) 10 x 4 (7.9)	32. 7.32-8.45 (M) 10 x 16 (3.5)
08	SDSSJ095014.05+580136.5	3.960	17.61	5.2 18.1-26.1 (H) 3 x 1 (24)	17. 5.37-6.99 (M) 10 x 4 (8.9)	24. 3.61-3.91 (L) 10 x 20 (3.5)
09	SDSSJ100129.64+545438.0	1.756	15.67	39. 18.8-27.0 (H) 3 x 1 (180)	84. 5.54-7.20 (M) 3 x 1 (13)	83. 3.30-3.60 (L) 10 x 3 (4.7)
10	SDSSJ101447.18+430030.1	3.126	16.39	17. 22.6-33.2 (H) 3 x 1 (79)	51. 6.86-9.05 (M) 3 x 2 (11)	63. 4.38-4.78 (L) 10 x 4 (4.2)
11	SDSSJ110610.73+640009.6	2.203	15.96	28. 16.5-22.1 (M) 3 x 1 (190)	69. 4.57-5.87 (M) 3 x 1 (10)	75. 3.19-3.44 (L) 10 x 3 (4.3)
12	SDSSJ111038.64+483115.6	2.955	16.53	15. 19.7-26.7 (H) 3 x 1 (70)	44. 5.94-7.29 (M) 3 x 2 (9.3)	54. 4.36-4.61 (L) 10 x 5 (4.)
13	SDSSJ121930.77+494052.3	2.699	16.79	12. 18.5-23.0 (M) 3 x 1 (83)	34. 5.31-6.24 (M) 10 x 1 (8.9)	40. 3.93-4.12 (L) 10 x 9 (4.)
14	SDSSJ123549.47+591027.0	2.825	16.71	13. 16.5-20.4 (M) 3 x 1 (90)	37. 4.53-5.56 (M) 10 x 1 (9.7)	44. 3.48-3.69 (L) 10 x 8 (4.1)
15	SDSSJ123641.46+655442.0	3.387	17.17	8. 15.3-19.7 (M) 3 x 1 (56)	25. 4.45-5.56 (M) 10 x 2 (9.2)	32. 4.98-5.20 (L) 10 x 15 (4.1)
16	SDSSJ135044.67+571642.8	2.906	16.92	11. 15.9-18.4 (M) 3 x 1 (77)	31. 4.26-5.02 (L) 10 x 1 (9.5)	37. 2.83-2.98 (L) 10 x 12 (4.2)
17	SDSSJ140747.22+645419.9	3.082	17.07	9. 14.4-17.7 (M) 3 x 1 (63)	27. 4.00-4.89 (L) 10 x 1 (8.3)	33. 3.40-3.58 (L) 10 x 14 (4.1)
18	SDSSJ142123.98+463317.8	3.363	17.22	7.6 17.6-18.7 (M) 3 x 1 (53)	24. 4.88-5.34 (M) 10 x 2 (8.9)	31. 3.67-3.77 (L) 10 x 15 (4.)

Observation Summary for MIPS (continued)

obj	Object Name	z	i (mag)	1st line: Estimated Flux Density (mJy) 2st line: Background (mJy/sr) (High/Medium/Low) 3rd line: Ramp Duration × Cycles (S/N) (24 μm)	(70 μm)	(160 μm)
19	SDSSJ142656.17+602550.8	3.192	16.22	19. 14.9-17.4 (M) 3 x 1 (130)	60. 4.10-4.93 (L) 3 x 1 (10)	75. 3.26-3.43 (L) 10 x 3 (4.3)
20	SDSSJ143835.95+431459.2	4.611	17.64	4.9 17.6-19.1 (M) 3 x 1 (34)	16. 4.94-5.49 (M) 10 x 4 (8.3)	25. 4.21-4.34 (L) 10 x 18 (3.5)
21	SDSSJ144542.75+490248.9	3.876	17.48	5.9 16.7-18.0 (M) 3 x 1 (41)	19. 4.80-5.40 (M) 10 x 3 (8.6)	26. 5.03-5.16 (L) 10 x 18 (3.6)
22	SDSSJ152156.48+520238.4	2.208	15.43	45. 15.3-17.5 (M) 3 x 1 (310)	112. 4.31-5.07 (L) 3 x 1 (19)	122 4.01-4.17 (L) 10 x 2 (5.7)
23	SDSSJ161434.67+470420.0	1.860	15.86	32. 14.4-17.7 (M) 3 x 1 (220)	71. 3.98-4.86 (L) 3 x 1 (12)	72. 3.26-3.44 (L) 10 x 3 (4.1)
24	SDSSJ162116.92-004250.8	3.703	17.24	7.4 25.7-41.6 (H) 3 x 1 (35)	24. 9.32-12.7 (H) 10 x 5 (8.5)	32. 13.6-14.3 (M) 10 x 16 (3.5)
25	SDSSJ170100.62+641209.0	2.735	15.89	28. 13.2-17.2 (M) 3 x 1 (190)	79. 3.88-4.92 (L) 3 x 1 (13)	93. 4.64-4.85 (L) 10 x 2 (4.3)
26	SDSSJ173352.22+540030.5	3.425	17.11	8.4 13.1-17.1 (M) 3 x 1 (58)	27. 4.10-5.04 (L) 10 x 1 (8.3)	34. 6.38-6.56 (L) 10 x 14 (4.2)
27	SDSSJ212329.46-005052.9	2.262	16.35	19. 27.0-47.8 (H) 3 x 1 (89)	48. 8.89-13.6 (H) 10 x 2 (11)	53. 7.26-8.16 (M) 10 x 8 (4.2)
28	HS1603+3820	2.510	15.89	29. 15.7-19.6 (M) 3 x 1 (200)	77. 4.31-5.35 (M) 3 x 1 (11)	88. 3.23-3.44 (L) 10 x 2 (4.1)

Note:— Flux density and background are estimated at the listed wavelengths. Please see Table 1 for our assessment of the background level (H/M/L). The i(mag) is the SDSS i-band magnitude. For HS1603+3820, it is chosen to be the same as that of one object with similar redshift and 2MASS magnitudes.

6 References

Becker, R. H., White, R. L., & Helfand, D. J. 1995, ApJ, 450, 559

Condon, J. J., Cotton, W. D., Greisen, E. W., Yin, Q. F., Perley, R. A., Taylor, G. B., & Broderick, J. J. 1998, *AJ*, 115, 1693

Gallagher, S. C., Richards, G. T., Lacy, M., Hines, D. C., Elitzur, M., & Storrie-Lombardi, L. J. 2007, *ApJ*, 661, 30

Dietrich, M., & Hamann, F. 2004, ApJ, 611, 761

Hines, D. C., Krause, O., Rieke, G. H., Fan, X., Blaylock, M., & Neugebauer, G. 2006, *ApJ*, 641, L85

Just, D. W., Brandt, W. N., Shemmer, O., Steffen, A. T., Schneider, D. P., Chartas, G., & Garmire, G. P. 2007, *ApJ*, 665, 1004

Lawrence, A. 1991, MNRAS, 252, 586L Maiolino, R., Shemmer, O., Imanishi, M., Netzer, H., Oliva, E., Lutz, D., & Sturm, E. 2007, *A&A*, 468, 979

Netzer, H., et al. 2007, *ApJ*, 666, 806

Richards, G. T., et al. 2006, *ApJS*, 166, 470

Schweitzer, M., et al. 2006, *ApJ*, 649, 79

Steffen, A. T., Strateva, I., Brandt, W. N., Alexander, D. M., Koekemoer, A. M., Lehmer, B. D., Schneider, D. P., & Vignali, C. 2006, *AJ*, 131, 2826

Shemmer, O., et al. 2006, ApJ, 644, 86

Shi, Y., et al. 2007, *ApJ*, 669, 841

Strateva, I. V., Brandt, W. N., Schneider, D. P., Vanden Berk, D. G., & Vignali, C 2005, AJ, 130, 387

Vestergaard, M. 2002, *ApJ*, 571, 733

7 Brief Resume/Bibliography

Michael S. Brotherton (Ph.D. 1996, University of Texas at Austin); Assistant Professor at the University of Wyoming; leads a group focused on multi-wavelength studies of quasars and star formation in quasars. Leads the Wyoming AGN group (http://physics.uwyo.edu/agn).
Zhaohui Shang (Ph.D. 2003, University of Texas at Austin); Research Scientist at University of Wyoming; PI of *Spitzer* quasar SED program (GO-2 #20084) and post-starburst quasar program (GO-3 #30075); Has extensive experience in multi-wavelength AGN studies.

- *Connections Between UV-optical and Mid-IR Properties in Quasars – Effects of Dust*

Shang, Z.; Brotherton, M.S.; Hines, D.C.; Dale, D., et al. 2007, ApJ, submitted.

Dean C. Hines (Ph.D. 1994, University of Texas at Austin); Research Scientist at the Space Science Institute; NICMOS/HST and MIPS/Spitzer Instrument and Science Team; Author/Co-author of 105 refereed publications on infrared astronomy (including 54 based in-part on Spitzer data), polarimetry, quasars, circumstellar disks, and evolved stars.

- *Spitzer Observations of High-Redshift QSOs*

Hines, D.C., et al. 2006, ApJ, 641, L85

- *HST Ultraviolet and Ground-based Optical Spectropolarimetry of IRAS QSOs: Dusty Scattering in Luminous AGNs*

Hines, D.C., et al. 2001, ApJ, 563, 512

Rajib Ganguly (Ph.D. 2002, Pennsylvania State University); Postdoc at the University of Wyoming; previous postdoc at STScI; Expert in research of quasar outflows.
Niel Brandt has 14 years of experience with X-ray and multi-wavelength studies of active galaxies; he has authored more than 150 papers on this subject. He leads a small research group at Penn State focused on active-galaxy studies and extragalactic surveys.
Ohad Shemmer has extensive experience in IR astronomy. He led several projects of ground-based near-IR spectroscopy of high-redshift quasars. Shemmer is the PI of *Spitzer* cycle 3 program #30476 (IRAC+MIPS photometry of weak-line quasars at high redshift).

- *Near-Infrared Spectroscopy of High-Redshift Active Galactic Nuclei. I. A Metallicity-Accretion Rate Relationship*

Shemmer et al. 2004, ApJ, 614, 547

Dennis Just is a graduate student at Steward Observatory working on galaxy evolution, and is the lead author of the paper (Just et al. 2007) where the sample of this proposal was originally defined.

- *The X-ray Properties of the Most Luminous Quasars from the SDSS*

Just, D.W.; Brandt, W.N.; Shemmer, O., et al. 2007, ApJ, 665, 1004

Sabrina Cales is a graduate student at the University of Wyoming, working with IRS data.

8 Status of Existing Spitzer Programs

Co-I Z. Shang is the PI of GO-2 program 20084 (joint Spitzer+HST program) – "Quasar Bolometric Luminosity and Spectral Energy Distributions from Radio to X-ray" – IRS data reduced; one paper submitted and refereed (Shang et al. 2007, ApJL).

Co-I Z. Shang is the PI of GO-3 program 30075 – "Unveil the Nature of Post-starburst Quasars" – One target pending IRS observation in cycle 4. IRS spectra partially reduced.

Co-I D. Hines is the PI of 3 GO 2 & 3 programs (Data 90%, Analysis 50%, Publications 1), one DDT program (Observations scheduled in December 2007); TC on 4 MIPS GTO programs (Data 100%, Analysis 70%, Publications 5) and 1 DDT program (Data 100%, Analysis 75%).

Co-I O. Shemmer is the PI of GO-3 program 30476 – "IRAC + MIPS Photometry of Weak-line Quasars at High Redshift" – paper in preparation (Shemmer et al. 2008).

9 Proprietary Period Modification

There are no modifications to the proprietary period.

10 Justification of Duplicate Observations

There are no duplicate observations.

11 Justification of Targets of Opportunity

There are no ToO observations.

12 Justification of Scheduling Constraints

There are no constraints on this program.